Frontiers of Environmental Science & Engineering
2025, 19(10): 135 https://doi.org/10.1007/s11783-025-2055-y

RESEARCH ARTICLE

Insight into the enhanced adsorption behavior and mechanism of ibuprofen from water on polyaniline/acid-impregnated reed biochar composite

Zhixian Zhou[1], Zhengxiang Li[1], Chenman Shi[1], Wenlong Zhang ✉ [1], Jiangtao Feng[3], Wei Yan[3], Hongjie Wang ✉ [1,2]

1. Hebei Key Laboratory of Close-to-Nature Restoration Technology of Wetlands, School of Eco-Environment, Hebei University, Baoding 071002, China
2. Engineering Research Center of Ecological Safety and Conservation in Beijing-Tianjin-Hebei (Xiong'an New Area) of Ministry of Education, Baoding 071002, China
3. Department of Environmental Science and Engineering, State Key Laboratory of Multiphase Flow in Power Engineering, School of Energy and Power Engineering, Xi'an Jiaotong University, Xi'an 710049, China

HIGHLIGHTS

- A new type of IBP adsorbent was prepared by *in-situ* polymerization.
- π–π and hydrogen bonding interactions are critical to adsorption.
- The effectiveness of N-doping for the adsorption of IBP was verified.
- The cost assessment results confirm the practical application potential.
- Regeneration and characterization confirm desorption agent enhance cycling stability.

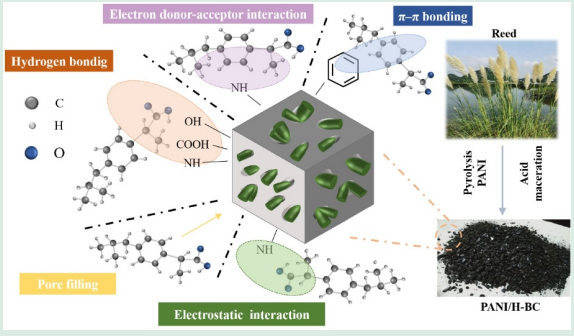

ABSTRACT: As a typical nonsteroidal anti-inflammatory drug, a significant amount of ibuprofen (IBP) can not be adsorbed by the human body and thus enters the environment, posing potential risks. Biochar (BC) adsorption is low-cost and easy to implement and is a potential technology for the removal of IBPs from water. To the best of our knowledge, the adsorption mechanism of IBP on BC is unclear, and certain physiochemical properties, such as low porosity, limit the adsorption capacity of IBP. In this study, a novel synthesis strategy involving the loading of nitrogen-rich polyaniline (PANI) particles is proposed to improve porosity and increase surface functional groups. A PANI/acid-impregnated reed BC (PANI/H-BC) composite was prepared through *in-situ* polymerization using reed BC synthesized via rapid pyrolysis. Adsorption experiments revealed that PANI/H-BC has a maximum adsorption capacity of 35.58 mg/g, which is 4.3 times and 3.7 times greater than those of PANI and BC, respectively. Besides, PANI/H-BC reached adsorption equilibrium within 30 min, reflecting a reduction of 50% compared to BC. It retains a significant adsorption capacity after ten cycles and is reusable. Moreover, the physical and chemical properties of PANI/H-BC were characterized, and the enhanced adsorption

✉ Corresponding authors. E-mails: zhangwenlong@hbu.edu.cn (W. Zhang); wanghj@hbu.edu.cn (H. Wang)
Article history: Received 21 February 2025, Revised 14 June 2025, Accepted 15 June 2025, Available online 15 July 2025

performance was demonstrated to be the result of multiple mechanisms, including π–π conjugation, hydrogen bonding and electrostatic interactions. These findings offer theoretical support for the adsorption and removal of IBPs as well as optimization of BC adsorbents. Production cost assessment and comparison, including industrial factors, were conducted. The low cost and renewability underscore its significant potential in practical applications.

KEYWORDS: Ibuprofen, Adsorption mechanisms, Biochar, Polyaniline, Rapid adsorption

1 Introduction

The production and consumption of pharmaceutical and personal care products (PPCPs) continue to be high on a global scale. However, most discharged PPCPs are overlooked in current urban water treatment policies, which leads to severe pollution. Among these PPCPs, IBP stands out as a chemical with high concentration, great potential risks, and wide distribution range in the environment (Dey et al., 2025). IBP, which serves as both an analgesic and an anti-inflammatory drug, is extensively utilized in the treatment of prevalent human ailments (Zhao et al., 2024). However, only 15% of the IBP used is absorbed by the human body, with the remaining 85% being excreted into the environment. Moreover, in the aftermath of the COVID-19 pandemic, the IBP concentration in water bodies significantly increased, which was attributed to the pandemic's impacts. In an ecotoxicological test conducted in 2014, IBP was demonstrated to impair the reproduction and development of aquatic animals (Ortiz de García et al., 2014). Reports have also shown that it disrupts the human immune system, leading to central nervous system disorders and intensifying organ dysfunction, potentially inducing compensatory hypogonadism in males (Yang et al., 2023b; Dey et al., 2025). Evidently, IBP poses a significant threat to both the natural environment and human health, necessitating its urgent removal from the environment. Guerra et al. (2014) conducted a study on six wastewater treatment plants (WWTPs) in Canada and reported that the detection rate of IBP was above 90% in all cases, with an average concentration reaching 8600 ng/L. As a result, IBPs cannot be completely removed in WWTPs, highlighting the need for the development of novel technologies or materials.

Over the past few decades, a surge in technological advancements has led to the development of numerous methods for removing IBP from water, including constructed wetlands, biodegradation processes, photocatalysis, electrochemical reduction, and adsorption techniques. Among these methods, adsorption technology stands out as one of the mature methods (Dey et al., 2025). It boasts low costs, high safety, and ease of implementation, while effectively removing nonsteroidal anti-inflammatory drugs (NSAIDs), including IBP, from water. Accordingly, compared with other methods, adsorption is considered a practical and feasible approach for treating IBP in water.

Adsorbent material selection is crucial for high adsorption efficiency. A recent review indicated that the predominant choice for adsorbents used in the uptake of IBPs from water is carbon-based adsorbents (Ayati et al., 2023). Among carbon-based adsorbents, BC is a low-cost and effective potential material. The porous structure and high affinity of BC for polar organic pollutants make it highly effective for removing organic contaminants (Xi et al., 2023). The functional groups on the surface of BC, including hydroxyl and carboxyl groups, also exhibit favorable pore structures, all of which contribute to its adsorption performance. However, the potential for further enhancement of the adsorption capacity is hindered by the limited porosity and specific surface area of raw BC. Functionalization can effectively remove pollutants from solution by enhancing their interactions. Through this special interaction, the stability between molecules is increased, and the electrostatic repulsion between charges is minimized, resulting in modified BC with a strong adsorption capacity. Show et al. (2021) utilized acid treatment to activate BC and demonstrated the effectiveness of acid modification.

Polymerization is an effective modification method. PANI has been widely studied for its ease of production and eco-friendly nature. Besides, the presence of large active sites, characterized by alternating benzene rings and nitrogen atoms in the main chain, significantly enhances adsorption chemistry. In addition, PANI demonstrates robust resistance to both acidic and alkaline environments, making it an ideal candidate for applications in water remediation and removal from anionic pollutants (Yang et al., 2022; 2023a; Huang et al., 2024). PANI consists primarily of micron-sized particles. Although it can not be melted for processing, it readily accommodates the addition of other materials

for molding. On this basis, PANI was chosen for incorporation into BC with the aim of enhancing its pore structure and increasing its porosity, facilitating the adsorption of IBPs. In addition, research conducted by Jung et al. (2015) confirmed that nitrogen-doped BC exhibited stronger adsorption effects toward IBP in a single-pollutant solution. In this study, the introduction of PANI into the material system is expected to combine the lone pair of nitrogen atoms with the anionic IBP complex, forming an electron donor–acceptor interaction. Research on the adsorption and removal of IBP using PANI/acid-impregnated reed BC (PANI/H-BC) is currently lacking, and the adsorption behavior and mechanism of IBP in water have not been revealed.

In this study, we analyzed the adsorption mechanism and evaluated the adsorption performance of PANI/H-BC for IBP from water. PANI/H-BC was prepared with an *in-situ* polymerization method. The adsorbent materials were characterized by scanning electron microscopy (SEM), nitrogen adsorption–desorption (BET), Fourier transform infrared spectroscopy (FTIR), X-ray diffraction (XRD), and X-ray photoelectron spectroscopy (XPS) before and after the adsorption of IBP. The analysis focused on the impact of various influencing factors, namely, contact time, pH, and adsorbate concentration, on the adsorption performance. Furthermore, the adsorption process was investigated by examining the adsorption kinetics models, isotherms, and reusability of the material. Finally, based on the results of the characterization and adsorption experiments, the mechanism of IBP adsorption onto the PANI/H-BC composite was thoroughly discussed and elucidated.

2 Experimental procedures

2.1 Materials

The reeds employed in this research were sourced from the Baiyangdian area of Hebei Province, China. Hydrochloric acid (HCl), methanol (CH_3OH) and aniline were obtained from Damao Chemical Reagent Factory (Tianjin, China). Ammonium persulfate was acquired from Shanghai Hutest Laboratory Equipment Co., Ltd., Shanghai, China. All chemicals and reagents utilized in this study were of analytical grade purity.

2.2 Synthesis of adsorbents

The BC and H-BC were obtained as follows. After washing with distilled water, the reeds were cut into segments of approximately 2 to 3 cm in length and subsequently placed within an oven, where they were heated at 80 °C until drying. The dried and screened biomass was then placed into a tube furnace under a nitrogen (N_2) atmosphere at different temperatures (400, 500, and 600 °C) for 30 min. After the sieving and washing processes, the BC samples were dried in an oven at 80 °C and thereafter labeled BC-400, BC-500, and BC-600. Afterward, the BCs were impregnated in 2 mol/L HCl solution for 24 h. Next, they were filtered and thoroughly washed with distilled water several times until the filtrate was neutral. The resulting modified BCs were designated H-BC-400, H-BC-500 and H-BC-600.

PANI was prepared by chemical oxidation polymerization. Precisely 47.2 g of HCl and 4.09 g of aniline were added to a glass beaker and mixed for an hour in an ultrasonic machine. Subsequently, 2.50 g of ammonium persulfate was slowly added dropwise to the mixture, which was dissolved in 40.0 mL of 2 mol/L HCl while stirring magnetically at a temperature of 0 to 5 °C for one hour. An ice water bath was used for cooling. After filtration, PANI was obtained by rinsing with distilled water multiple times. The as-prepared samples were dried at 80 °C for 24 h and then sieved through a 50-mesh screen. The powders obtained are denoted as PANI.

The PANI/H-BC samples were synthesized through the process of *in-situ* polymerization of PANI within a solution containing H-BC. Following a typical preparation procedure, 1 g of H-BC, 47.2 g of HCl and 4.09 g of aniline were added to a glass beaker and mixed for an hour in an ultrasonic machine. Similarly, a mixture comprising 40.0 mL of 2 mol/L HCl and 2.5 g of ammonium persulfate was slowly introduced, while immersed in an ice bath. After filtration, washing, drying and sieving, the resulting PANI/H-BC samples were labeled PANI/H-BC-400, PANI/H-BC-500 and PANI/H-BC-500. As shown in Text S1 and Fig. S1 (Supporting Information), H-BC-500 and PANI/H-BC-500 exhibited better adsorption performances than the other two samples did. Accordingly, H-BC-500 and PANI/H-BC-500 were used as the main BC samples in the following adsorption process. For simplification, H-BC-500 and PANI/H-BC-500 are abbreviated as H-BC and PANI/H-BC, respectively, in the following discussion.

2.3 Analysis and characterization methods

In this study, the microstructure and morphology were characterized by SEM (ZEISS GeminiSEM 300,

Germany). The specific surface area and pore volume of the adsorbents were determined by BET (Micromeritics ASAP 2460, USA) with N_2 adsorption and desorption isotherms. In addition, the functional groups present in the various materials were detected by FT-IR (Thermo Scientific Nicolet iS50, USA). The chemical state and surface composition were obtained by XPS (Thermo Scientific ESCALAB 250Xi, USA). The structure and crystallinity of the materials were analyzed using X-ray diffraction (XRD, Rigaku SmartLab SE, Japan). The zeta potential was determined utilizing dynamic light scattering (Malvern Zetasizer Nano ZS90, Britain). Furthermore, a contact angle/surface tension meter (Kunshan Chengding SDC 350KS, China) was used to measure the contact angle between the adsorbents and solution. The surface roughness of the material was determined by atomic force microscopy (AFM, Bruker Dimension iconXR, USA).

2.4 Adsorption experiments

The concentration of IBP was determined using a UV–VIS spectrophotometer (Persee TU1900, China) at a wavelength of 224 nm, as shown in Text S2 and Fig. S2. All the adsorption experiments were conducted at 25 °C. To investigate the effects of pH on adsorption performance, the pH of the 20 mg/L IBP solution was adjusted from 3 to 13 using HCl and NaOH solutions with an adsorbent dosage of 2 g/L. For kinetic studies, 0.4 g of adsorbent was added to 200 mL of 20 mg/L IBP solution, which reached adsorption equilibrium after 5 h. Isothermal adsorption experiments were performed by mixing 40 mg of adsorbent with 20 mL of IBP solutions with initial concentrations ranging from 2 to 30 mg/L. To examine the influence of coexisting substances, either 0.01 mol/L inorganic ions or 20 mg/L organic compounds were introduced into the IBP solutions. Additional details regarding the adsorption experiments are presented in Text S3.

2.5 Desorption and regeneration experiments

To desorb IBP from the adsorbent, a mixed solution of ethanol and 0.01 mol/L NaCl was employed. After each adsorption cycle, the adsorbent was immersed in this desorbing solution for 30 min, followed by multiple rinses with distilled water and drying. The reusability of PANI/H-BC and the efficacy of the desorption agents were evaluated through ten desorption cycles.

3 Results and discussion

3.1 Adsorbent characteristics

The SEM images corresponding to PANI/H-BC, PANI and H-BC are shown in Figs. 1(a)–1(c). Inspection revealed that H-BC has a relatively smooth surface with a limited number of relatively large pores. In contrast, the surface morphology of the modified BC composite, PANI/H-BC, is like that of PANI, displaying a distinctive porous network-like fibrous structure with irregular surfaces and pronounced pore sizes. According to the AFM results, the root mean square roughness (Rq) of PANI is 0.971 nm, whereas the Rq of PANI/H-BC increases to 133 nm after loading, indicating successful incorporation of PANI. This is

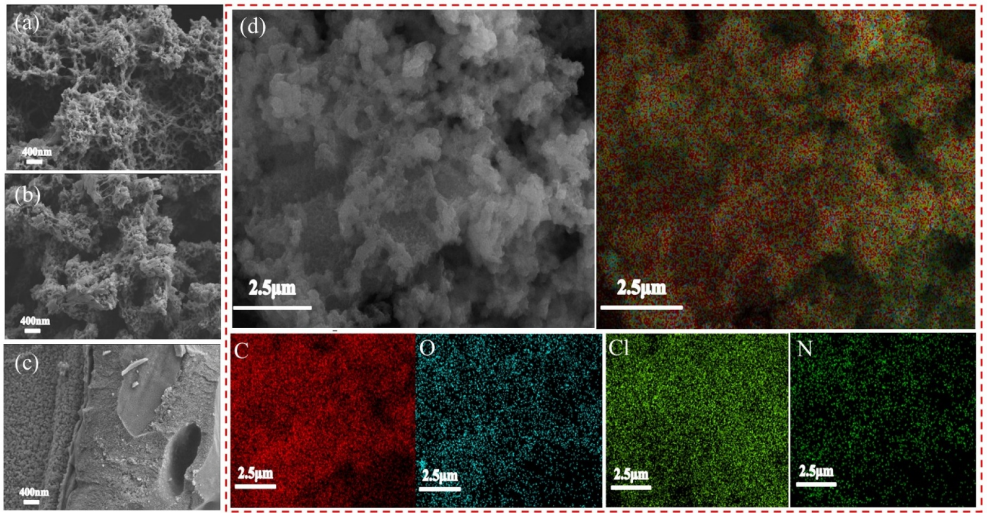

Fig. 1 SEM images of (a) PANI/H-BC, (b) PANI, (c) H-BC, and (d) elemental mapping of PANI/H-BC.

also confirmed by element mapping, as shown in Fig. 1(d). Compared with the PANI/H-BC composite, the PANI/H-BC composite has a smaller particle size and greater surface roughness and porosity. The formation of this porous structure and rough surface provides more active sites, thereby enhancing the adsorption capacity. Furthermore, the distribution of elements and their respective mapping images across the surface of the PANI/H-BC are shown in Fig. 1(d). The results indicate that the prepared adsorbent surface is widely distributed with elements such as C, O, N, and Cl.

According to the elemental content results in Table 1, significant differences exist among the as-prepared adsorbents. The N content in PANI/H-BC significantly exceeds that in H-BC, due to the formation and precipitation of PANI particles because of the oxidative polymerization of aniline in the solution. The increase in Cl content is likely due to the incorporation of counter-anions generated from the decomposition of doped protonic acids into the main chain. Therefore, it forms polarons and bipolarons that delocalize into the π-bonds of the entire molecular chain by binding with N atoms in the amine and imine groups (Zhang et al., 2024). In addition, the increase in the N and Cl contents in the PANI/H-BC composite confirmed successful *in-situ* polymerization. Since the surface of reed stems possesses a waxy layer rich in silicon and fatty substances, the Si content in H-BC is notably high. After modification by PANI, a substantial reduction in the Si content is observed, presumably attributed to the removal of most of the silica scaling during low-temperature polymerization. Studies have shown that excessive oxygen content on the surface may occupy defect sites on the BC surface, thereby affecting the adsorption performance (Ren et al., 2020). As a result, the decrease in surface oxygen content after loading might be beneficial for the IBP adsorption process.

Table 1 Physical-chemical properties of PANI/H-BC, PANI and H-BC by BET, SEM mapping and zeta potential tests

Analysis/Properties	PANI/H-BC	PANI	H-BC
S_{BET} (m^2/g)	10.567	18.604	8.763
V (cm^3/g)	0.052	0.102	0.014
R (nm)	19.523	21.951	6.555
C (w%)	74.78	72.54	70.64
N (w%)	13.26	14.65	0.17
O (w%)	6.7	3.21	21.23
S (w%)	1.01	1.29	0.04
Cl (w%)	3.78	4.9	0.84
Si (w%)	0.17	0.06	6.43
Zero potential charge (pH_{pzc})	3.8	4.8	4.85

The physical properties of adsorbents, such as pore structure, specific surface area and pore size distribution, are intricately linked to the surface adsorption process. The specific surface area (S_{BET}), pore volume (V), and average pore radius (R) of the adsorbent samples were calculated and are presented in Table 1. Additionally, the adsorption–desorption isotherms and pore size distribution curves are depicted in Figs. S3(a)–S3(c). Based on the International Union of Pure and Applied Chemistry (IUPAC) classification, the N_2 adsorption–desorption curves of all adsorbents exhibited Type III adsorption isotherm behavior. This suggests that the pores within the structure consist primarily of mesopores and macropores. In addition, the quantity of pores is relatively small. As a result, it is well suited for multimolecular layer adsorption. The non-closure of the N_2 adsorption–desorption isotherm curve of H-BC could be attributed to the reduction in the flexible pore diameter after gas adsorption, hindering gas desorption.

As shown in Table 1, the values of S_{BET}, V and R of PANI/H-BC are significantly greater than those of H-BC. The effect of loading PANI onto the BC surface, which changed the morphology from smooth and flat to loose and porous, might be the main contributor to these results. This change in surface area and pore properties is anticipated to enhance the IBP adsorption. Through calculations, we determined that the S_{BET} of PANI was 18.604 m^2/g, with a V of 0.102 cm^3/g and an R of 21.951 nm. However, upon loading, these values slightly decreased, presumably because of the interference of H-BC during the deposition process of PANI.

As illustrated in the XRD patterns in Fig. 2(a), the diffraction pattern of H-BC displays a single peak at 2θ = 22.85°, corresponding to the graphite structure plane of BC. This indicates a certain degree of graphitization in reed BC (Zhang et al., 2018). Additionally, a weak SiO_2 diffraction peak is detected at 2θ = 28.30°, suggesting that after acid impregnation, most of the metallic impurities of the reed BC have been removed, leaving only a small amount of quartz crystal components. Compared with H-BC, PANI has a greater number of diffraction peaks. The diffraction peaks at 2θ = 9.39°, 14.73°, 20.38°, and 25.18° can be indexed to the (0 0 1), (0 1 1), (0 2 0) and (2 0 0) crystal plane diffractions of PANI (Liu et al., 2023). The two prominent broad peaks located at 2θ = 20.38° (0 2 0 plane) and 25.18° (2 0 0 plane) signify the repetitive arrangement of benzene rings and quinone rings. These peaks are attributed to the presence of polymer chains

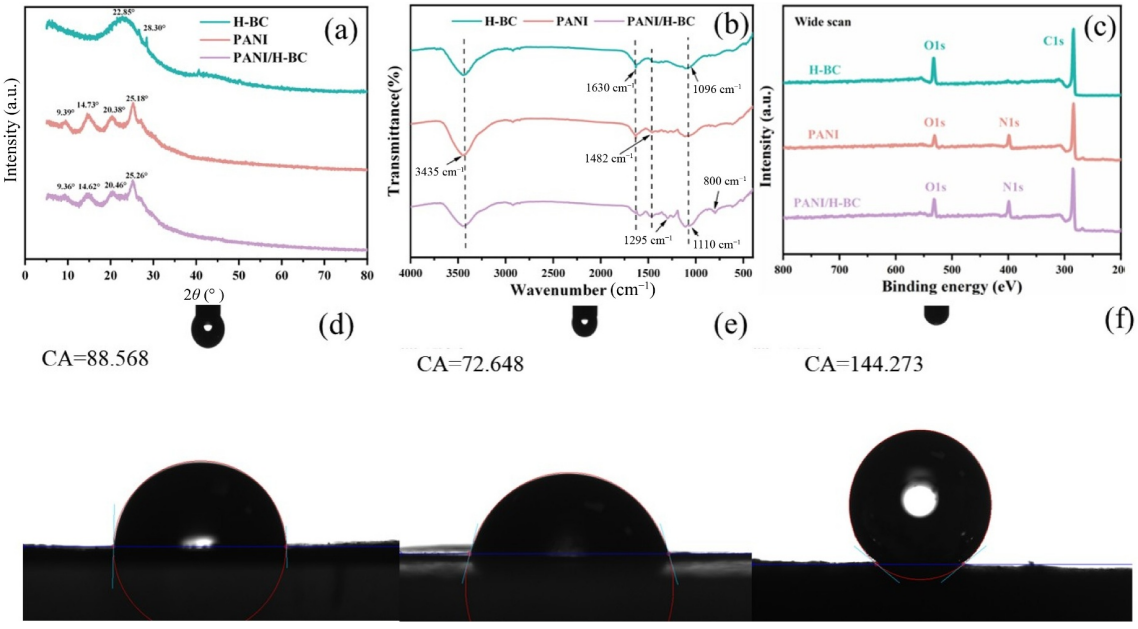

Fig. 2 (a) XRD patterns of PANI/H-BC, PANI and H-BC; (b) FTIR spectra of PANI/H-BC, PANI and H-BC; (c) XPS survey scan spectra; contact angle measurement diagrams of (d) PANI/H-BC, (e) PANI, and (f) H-BC.

that are oriented either parallel or perpendicular to each other (Yea et al., 2022; Liu et al., 2023). Furthermore, Fig. 2(a) shows that the crystallinity of BC significantly improved after loading with PANI. The presence of characteristic peaks can be observed in the hybrid adsorbents, which confirms the successful preparation of the PANI/H-BC composite using in-situ oxidative polymerization. Moreover, the peaks corresponding to PANI broaden and shift in PNAI/H-BC, which may be attributed to the hindrance of aniline polymerization caused by the addition of BC.

The FTIR spectra corresponding to PANI, H-BC and PANI/H-BC are displayed in Fig. 2(b). The numerous functional groups present in H-BC and PANI may serve as effective sites during the modification process and contribute to the structural alterations of the prepared adsorbents. The characteristic bands of H-BC located at 3435 and 1630 cm^{-1} are associated with the tensile vibrations of −OH and C=C, respectively. In addition, the peak at 1096 cm^{-1} is assigned to the bending vibration of C=O, which emerges because of the carboxylation process undergone by BC under the catalytic effect of protonic acids. The occurrence of C=O and C=C bonds may facilitate the adsorption of organic molecules via oxygen-containing functional groups and π–π interactions (Guo et al., 2024). The primary vibration peaks of PANI are predominantly observed at 3435, 1630, 1482, and 1110 cm^{-1}. These peaks are attributed to O−H stretching vibrations, quinone groups in PANI, and C=C stretching vibrations in the benzene ring skeleton. The peak observed at 1110 cm^{-1} corresponds to the stretching vibration of $-NH^{+}=$ in the two forms of PANI (Wang et al., 2013). Upon investigation, the FTIR spectrum of the PANI/H-BC composite exhibited distinct peaks that were characteristic of the original materials, unequivocally indicating the successful integration and loading of the components. After modification, the relative intensity of the O−H vibration peak at 3435 cm^{-1} decreases, whereas the peak intensity at 1110 cm^{-1} increases significantly. An additional peak appears at 1295 cm^{-1} in the spectra. The enrichment of C−O and C−N bonds in the modified material can be attributed to the incorporation of protonated amino groups. This increase in the chemical composition suggests a meticulous and effective modification process, leading to a composite with enhanced functional properties. Furthermore, a sharp peak appearing at 800 cm^{-1} belongs to the out-of-plane C–H stretching vibration. The absorption peak at 1630 cm^{-1} is less pronounced in the composite sample than in H-BC, likely resulting from the condensation reaction between amine groups and carboxylic acids on H-BC. Amide groups can effectively bridge particles, forming flocculated clumps through hydrogen bonding with oxygen atoms on the IBP surface. This phenomenon highlights the considerable potential for both adsorption and sedimentation.

The contact angle plays a vital role in determining the wettability characteristics of a liquid on a given

material's surface. Specifically, if the contact angle is less than 90°, the solid surface is hydrophilic; otherwise, it is hydrophobic. Accordingly, the hydrophilicity and hydrophobicity of the adsorbent materials were evaluated with the contact angle measurements, as depicted in Figs. 2(d)–2(f). Upon observation, the contact angles of H-BC and PANI/H-BC were determined to be 144.273° and 88.568°, respectively. Indeed, after the loading of PANI, the surface of the BC adsorbent underwent a transformation from hydrophobic to hydrophilic. To the best of our knowledge, the pK_a of IBPs is 4.91. When the solution pH exceeds the pK_a value, IBP is hydrophilic (Bui and Choi, 2009). The modified adsorbent exhibited improved dispersion and stability in aqueous solutions, thereby increasing the contact area with IBP molecules and enabling more effective interactions with IBPs. Thus, when the pH conditions are optimal, the process of IBP adsorption in an aquatic setting becomes particularly favorable.

To determine the molecular structure of the adsorbent, XPS analysis was performed on the prepared samples. An exhaustive analysis of the binding energies of the samples was conducted, and the findings from this analysis are depicted in Fig. 2(c). The binding energies of C, O, and N reached peak values of 284, 530, and 398 eV, respectively. Notably, after loading, PANI/H-BC displayed a significant N1s peak, which aligns with the SEM findings and indicates the successful synthesis of the composite material.

3.2 Effect of pH

The pH of the solution is a crucial factor affecting the adsorption efficiency, as it directly influences the surface charge and degree of ionization of both the adsorbents and IBP. Figures 3(a)–3(c) present the adsorption capacities of IBP onto H-BC, PNAI and PANI/H-BC across a range of pH values from 3.0 to 13.0. Notably, all the adsorbents exhibit a significant adsorption capacity for IBP within a broad pH range of 3.0 to 9.0, potentially owing to the stability of IBP within this pH range.

The adsorption performance of H-BC for IBP is

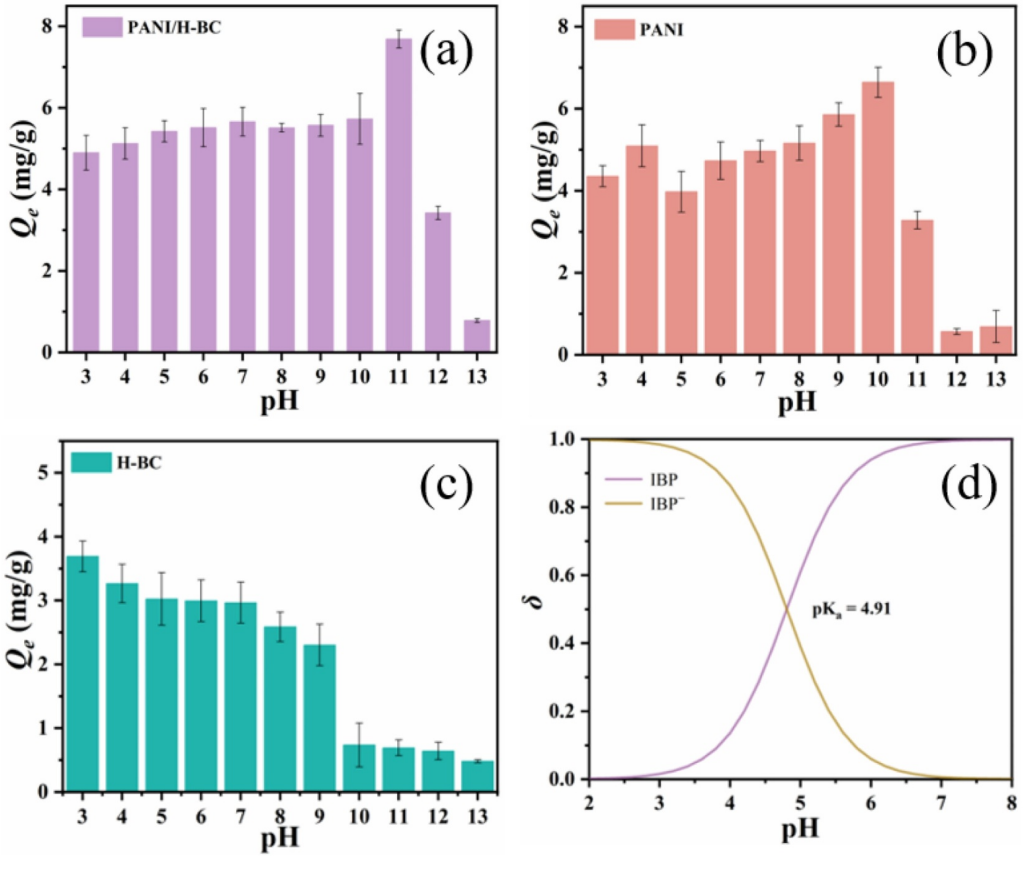

Fig. 3 Effect of pH on the adsorption capacity of (a) PANI/H-BC, (b) PANI and (c) H-BC; (d) the presence of IBP at different pH values.

significantly greater under acidic conditions than under alkaline conditions, and H-BC adsorption capacity decreases with increasing pH. The observed result can be explained by considering the pH_{pzc} of H-BC and the pK_a of IBP. Figure 3(d) shows that at a pH of 2.0, IBP predominantly exists in its molecular form, accounting for more than 99% of all IBP. As the pH exceeds 4.0, IBP starts to progressively acquire an anionic form. At pH = 7.0, more than 99% of IBP exists predominantly in its anionic form (Mondal et al., 2016). As shown in Table 1, the pH_{pzc} of H-BC is 4.85. The surface of H-BC is positively charged under strongly acidic conditions and gradually becomes negatively charged as the pH increases. The experimental results show that non-ionized IBP strongly interacts with the surface of H-BC, provided that the pH of the solution is lower than the pK_a value of IBP.

Bare PANI has better adsorption performance in alkaline media than in acidic solutions. At a pH of approximately 10, the protonic imine groups undergo deprotonation, resulting in nitrogen atoms with lone pairs, which can provide electron pairs to conjugate with the anionic IBP complex and form electron donor-acceptor interaction (Rafiqi and Majid, 2017). Consequently, they exert an attractive force on the IBP. However, when the pH is excessively high, electrostatic repulsion between the adsorbent and IBP becomes predominant, causing a notable decrease in absorptive power. When the pH reaches 4.0, the adsorbent surface acquires a gradual positive charge as the imine and amine groups undergo protonation. The electrostatic interaction and adsorption performance for anionic IBP are thus enhanced (Wang et al., 2013). The effect of pH on PANI/H-BC follows a similar trend to that on PANI. Accordingly, it is hypothesized that electron donor-acceptor interactions and hydrogen bonding contribute significantly to adsorption under alkaline conditions. In addition, the coexisting ions competed with IBP for adsorption sites, binding with water molecules and weakening the hydrogen bonding between IBP and water. This reduced IBP solubility, promoting diffusion onto PANI/H-BC and increasing its adsorption (Schlautman et al., 2004). Evidently, PANI/H-BC has a greater affinity for IBP adsorption than H-BC and PANI across the entire pH range studied. Therefore, depositing PANI on the surface of H-BC proves to be an effective strategy for increasing its adsorption capacity for IBP.

The investigation of the effects of pH on adsorption performance should not be limited to single-point conditions but should comprehensively consider the synergistic influence of pH and concentration. As shown in Fig. S4, the adsorption capacity progressively increased with increasing initial IBP concentration, which can be attributed to the increased mass transfer driving force. Furthermore, the adsorption performance at pH = 11 was comprehensively superior to that at pH = 3 and pH = 7, validating the reliability of the pH experimental results.

3.3 Effects of co-existing organic substances and ions

Natural water may contain various coexisting organic substances and competitive ions, which can influence the adsorption of pollutants. In this study, the effects of humic acid (HA), bisphenol A (BPA), rhodamine B (RB), and coexisting ions (Ca^{2+}, Mg^{2+}, SO_4^{2-}, and CO_3^{2-}) on the adsorption removal of IBP by PANI/H-BC were investigated. As shown in Fig. S5, BPA and HA facilitated the adsorption of IBP. This enhancement can be attributed to the abundant hydroxyl groups and π-electrons in BPA and HA, which promote the formation of hydrogen bonds and π–π interactions (Luo et al., 2023). The addition of CO_3^{2-} caused a significant reduction in adsorption, likely due to an increase in solution pH, leading to a decrease in the positive surface charge of the adsorbent and weakening the electrostatic attraction with IBP. The slight inhibitory effects of Ca^{2+} and Mg^{2+} may result from their complexation with the carboxylate group of IBPs, reducing the adsorption driving force. Moreover, the inhibition by SO_4^{2-} could be attributed to limited competitive adsorption with IBPs (Li et al., 2018).

3.4 Adsorption kinetics

Understanding adsorption kinetics, particularly the rate at which equilibrium is reached, is crucial for designing effective adsorption systems. In this study, two kinetic models (the pseudo-first-order kinetic model and the pseudo-second-order kinetic model) were applied to predict the primary process occurring between the adsorbents and IBP, as well as to estimate the adsorption rate. The suitability of the kinetic models for describing the adsorption process was evaluated using the coefficient of determination (R^2).

The fitting curves and parameters are presented in Fig. S6 and Table S1. IBP adsorption onto PANI/H-BC exhibited rapid initial adsorption, followed by a slower increase in capacity. This is presumably attributed to the high initial availability of adsorption sites. Subsequently, equilibrium is reached after approximately 30 minutes, as the active sites become increasingly saturated. This highlights the remarkable advantage of the PANI/H-BC powder material in achieving a rapid adsorption rate for IBP in water.

The IBP adsorption process better fits the pseudo-second-order kinetic model (R^2 = 0.9726) than the pseudo-first-order model (R^2 = 0.9116), suggesting that chemical adsorption is the dominant mechanism. Based on this assumption, the rate-limiting step may be dominated by hydrophobic interactions and hydrogen bonding forces between PANI/H-BC and IBP. The adsorption of PANI, like that of IBP, conforms well to the pseudo-second-order kinetic model. In contrast to PANI/H-BC, PANI also exhibited a good fit with the pseudo-first-order kinetic model, suggesting a significant contribution of physical adsorption to IBP uptake. The equilibrium adsorption capacity of PANI/H-BC was determined to be 8.3484 mg/g using the pseudo-second-order kinetic model, which closely matches the experimental value of 8.5923 mg/g. In addition, the adsorption capacity of the three adsorbents followed a pattern of PANI/H-BC > PANI > H-BC.

3.5 Adsorption isotherms

Adsorption isotherms provide insights into the interactions between adsorbents and adsorbates. The adsorption isotherm data at 298 K were fitted to three vital models: the Langmuir, Temkin and Freundlich models. The fitting results are presented in Fig. S7 and Table S2. A positive correlation was observed between the adsorption capacity of the adsorbents and the initial concentration of IBP in the aqueous solution. This phenomenon is likely driven by the increasing concentration gradient between the adsorbent particles and the solution. The greater driving force for mass transfer could increase the efficiency with which the adsorbent material attracts IBP to its surface.

The fitting curves and high correlation coefficients (R^2) indicate that the Langmuir model best describes the adsorption process, suggesting monolayer adsorption on the PANI/H-BC surface and a homogeneous adsorption mechanism. The Langmuir model calculation reveals a significantly enhanced maximum adsorption capacity of 35.5758 mg/g for PANI/H-BC at 298 K, representing a 4.3-fold increase compared with that of PANI and a 3.7-fold increase compared with that of BC. The fitted values for $1/n$ in the Freundlich model, which represent the adsorption intensity, are all less than 1. This suggests that adsorption is favorable and is associated with a relatively high binding constant (K_L). In addition, the Temkin model parameter b is a measure of the heat of adsorption. The positive values of b indicate the exothermic property of the process, whereas the lower adsorption heat of PANI/H-BC suggests that less energy is required for adsorption.

The Freundlich model demonstrated the highest correlation with the experimental data for IBP adsorption onto BC, as evidenced by an R^2 value of 0.9787. Compared with the Freundlich and Temkin models, the Langmuir model, with an R^2 of 0.99, best describes IBP adsorption onto PANI. As a result, the isothermal data support the kinetic findings, indicating that PANI/H-BC has a demonstrably higher adsorption rate and capacity for IBP than the other samples.

From a comprehensive view of the adsorption capacity and equilibrium time, as shown in Fig. 4, PANI/H-BC has emerged as a highly economical and efficient adsorbent, exhibiting significant advantages in the adsorption of IBPs from aquatic environments.

3.6 Adsorption mechanism

It can be seen that the adsorption efficiency of IBP on adsorbents is affected by both electron donor-acceptor interaction and electrostatic interactions. In addition, the pores in the adsorbent exist mainly in the form of mesopores and macropores, which helps to enhance the pore filling effect.

To elucidate the mechanism of IBP adsorption, XPS analysis was conducted to investigate the chemical states and compositional evolution of the elements in the adsorbent structure before and after adsorption. As shown in Fig. 5(a), the deconvoluted N1s spectrum of the PANI/H-BC composite reveals three characteristic peaks at binding energies of 399.04, 400.64, and 402.27 eV, corresponding to neutral amine (−NH−), positively charged polaron nitrogen, and bipolaron nitrogen species, respectively (Herath et al., 2021). Notably, the peak intensity of positively charged nitrogen increases after adsorption. This is due to interactions between

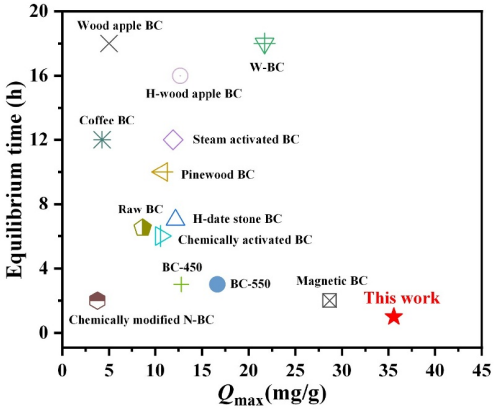

Fig. 4 Comparison of the maximum IBP removal capacity of various BCs. Data from references Mondal et al. (2016); Lin et al. (2017); Chakraborty et al. (2018a; 2018b).

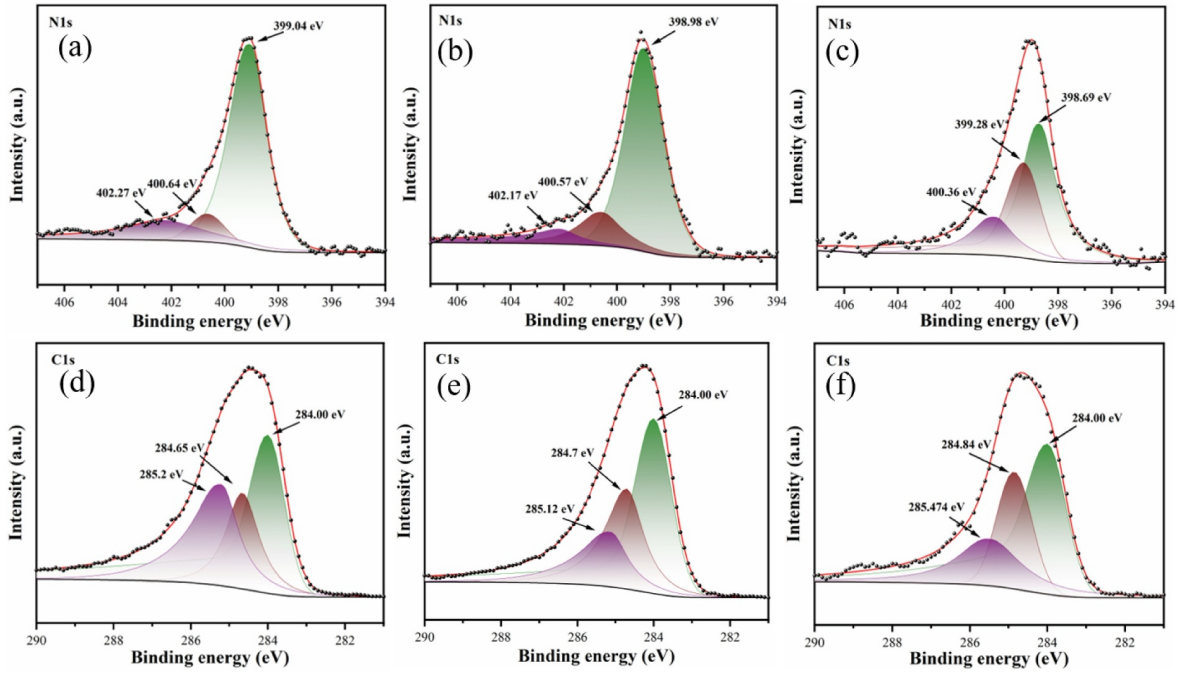

Fig. 5 XPS N1s spectra of PANI/H-BC (a) before adsorption, (b) after adsorption, (c) after desorption and XPS C1s spectra of PANI/H-BC (d) before adsorption, (e) after adsorption, (f) after desorption.

carbonyl groups and nucleophiles such as amines, which occur easily in both ground and excited states. These interactions could lead to the doping of PANI, resulting in the formation of positively charged nitrogen, thereby enhancing the affinity of PANI for IBP (Golovina et al., 2008). The reduction in the peak intensity of bipolaron may be attributed to the electrostatic interaction between protonated PANI/H-BC and IBP, which is consistent with the analysis in the literature (Herath et al., 2021).

Figure 5(d) displays the high-resolution C1s spectrum of the pristine adsorbent, which is deconvoluted into three peaks centered at 284.00 eV (C=C), 284.65 eV (C−C), and 285.2 eV (C−N). The existence of C=C and C−C bonds implies a highly hydrophobic surface with conjugated π regions on the BC (Navarathna et al., 2019). The shifts in the C1s binding energy highlight the pivotal role of carbon in IBP adsorption. For example, the significant decrease in the C–N peak intensity after adsorption suggests the involvement of hydrogen bonding (Mei et al., 2021). Furthermore, variations in the C–C peak intensity indicate the substantial impact of π–π interactions between the aromatic rings of the PANI/H–BC and IBP molecules.

A comparative FTIR analysis of the three adsorbents before and after IBP adsorption was conducted to further validate the hypotheses regarding the adsorption mechanism. The result is illustrated in Fig. 6.

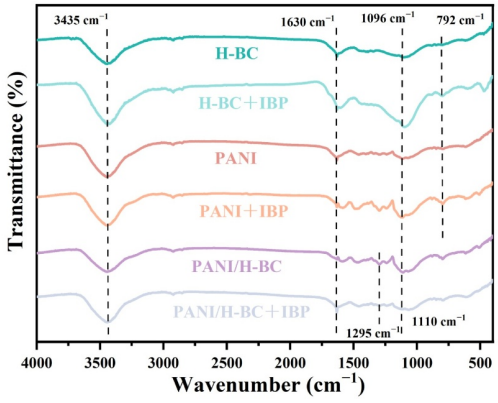

Fig. 6 FTIR spectra of PANI/H-BC, PANI and H-BC before and after adsorption.

Evidently, the peak intensities at 1295 and 1110 cm^{-1} significantly decrease following adsorption, indicating that C=C, C−N, and $-NH^{+}=$ play crucial roles in the adsorption process. This finding aligns with the results obtained from the XPS analysis. Simultaneously, the characteristic peaks are associated with the composite material shift after adsorption. This is presumably due to the π–π interactions between the benzene ring of IBP and the aromatic rings of PANI/H-BC. The increase in peak intensity and the shift observed at 1630 cm^{-1} are indicative of hydrogen bonding (Xiong et al., 2019). Notably, the increase in peak intensity at 3435 cm^{-1}

after IBP adsorption suggests that competition for adsorption sites occurs between water molecules and IBPs. This competition results in much moisture on the material surface after adsorption, which is also observed in H-BC.

The significant broadening of the peak at 1096 cm^{-1} after IBP adsorption onto H-BC and PANI indicates strong hydrogen bonding interactions. Furthermore, the presence of a weak peak at 792 cm^{-1}, characteristic of the out-of-plane bending vibration of C–H bonds, may suggest a π–π electron donor–acceptor interaction between the material surface and protonated IBP. These results imply that the adsorption mechanism is predominantly governed by a combination of hydrogen bonding, π–π electron donor–acceptor interactions, and hydrophobic effects.

In summary, the adsorption of IBP onto PANI/H-BC is the result of multiple coupled mechanisms (Fig. 7). Among them, the π–π interactions between benzene rings, as well as the hydrogen bonding interactions that act on the surface oxygen of IBPs, play dominant roles. Additionally, owing to the mesoporous structure of the adsorbent, pore filling effects also contribute to the adsorption process. Moreover, the electrostatic interactions and electron donor–acceptor interactions between the anionic IBP complex and the lone pair of nitrogen atoms also influence the adsorption efficiency.

3.7 Regeneration tests

Adsorbent materials are required to maintain a high adsorption capacity after continuous adsorption and desorption cycles, which is crucial for practical applications. As depicted in Fig. S8, the experiments revealed a gradual decline in the removal efficiency with repeated desorption. Remarkably, the adsorbent still has an adsorption capacity of 10.86 mg/g after ten cycles, underscoring its notable reusability. This reusability not only offers cost-effectiveness but also augments its application potential. Additionally, the decrease in the adsorption capacity of PANI/H-BC following repeated adsorption–desorption cycles can be attributed to material wear, which leads to a decrease in the number of available active adsorption sites.

To delve deeper into the causes of the reduced adsorption efficiency, quantitative functional group analysis of the regenerated adsorbent was conducted.

The effective regeneration of the PANI/H-BC adsorbent was systematically verified through FTIR analysis. As shown in Fig. S9, the intensities of the characteristic peaks at 1295 and 1110 cm^{-1} after regeneration were comparable to those of the original adsorbent, confirming the regeneration success. Nevertheless, following multiple regeneration cycles, a surge and shift in the peak intensity at 1630 cm^{-1} were noted. It is hypothesized that incompletely desorbed IBP molecules occupy the active sites via hydrogen bonding, thereby contributing to capacity degradation. This proves the pivotal role of hydrogen bonding in the adsorption mechanism. Furthermore, the pronounced increase in the peak intensity at 1380 cm^{-1} is presumably due to the interference of residual ethanol trapped within the pores of the adsorbent (Mondol et al., 2022).

XPS analysis of the regenerated adsorbent, as shown in Fig. 5(f), revealed an increased peak intensity for the

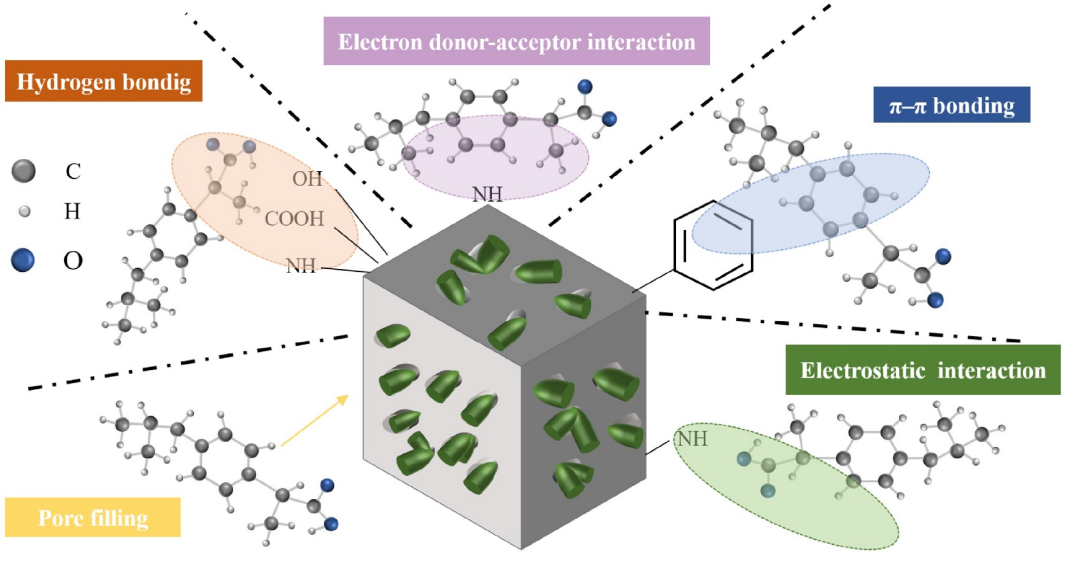

Fig. 7 Adsorption mechanism for the uptake of IBP onto PANI/H-BC.

C–C bond. This is likely attributed to incomplete IBP desorption. The single-bond structure in IBP enhances the C–C peak intensity, suggesting a gradual decrease in adsorption capacity upon repeated use. In the N1s spectrum, distinct peak shifts and intensity enhancements of polaron states were observed. This could result from ethanol, a protic solvent, facilitating the formation of more stable doped states in PANI, thereby increasing the electron density around nitrogen atoms and reducing their binding energy (Zhang et al., 2024). Additionally, ethanol may partially convert highly oxidized bipolarons to polarons, which also contributes to the bipolaron peak shift. The bipolaron peak shift toward a lower binding energy reduces oxidative damage in PANI, thereby enhancing cycling stability. These observations validate the scientific value of the desorption agent (Shyamala et al., 2022).

The BET test was conducted on the regenerated adsorbent to monitor the structural integrity of the material, as shown in Fig. S3(d). The specific surface area, pore volume and pore diameter of the material decreased in a coordinated manner. The specific surface area decreased from 10.58 to 8.97 m^2/g. It is speculated that multiple cycling experiments may have caused the collapse of the pores on the material surface. Although irreversible structural damage occurred, the material maintained a significant adsorption capacity even after ten regeneration cycles, demonstrating its practical applicability. Moreover, the ecotoxicity of the adsorbent was evaluated as demonstrated in Text S4, thereby further enhancing the discussion of its sustainability.

3.8 Economic feasibility

The economic cost of the prepared material is crucial for its practical application. As summarized in Table 2, the PANI/H-BC adsorbent demonstrates exceptional cost-effectiveness, with a production cost of 2.991 USD/kg. In this research, under optimal conditions, 2 g/L PANI/H-BC is capable of effectively removing 20 mg/L IBP solution, resulting in a wastewater treatment cost of only 0.003 USD/L. This result represents a cost reduction compared with that of the conventional biomass-derived adsorbents listed in Table S3. Notably, this adsorbent can be regenerated and reused at least 10 times without significant loss of removal efficiency, thereby further reducing the total life-cycle cost.

Techno-economic analysis as shown in Table S4, reveals a comprehensive process cost of 0.00184 USD/L, establishing quantifiable feasibility for industrial-scale implementation. The combination of low production costs and excellent regenerative capabilities positions PANI/H-BC as a highly competitive and promising adsorbent for practical applications.

4 Conclusions

In this study, a novel mesoporous adsorbent, PANI decorated H-BC from reed biomass feedstock, was successfully synthesized for the adsorption of IBP using the *in-situ* polymerization method. The as-obtained composite PANI/H-BC was thoroughly characterized using various analytical techniques. The comprehensive results confirmed the successful modification of PANI on the surface of H-BC and highlighted the superiority of the PANI/H-BC composites in terms of functional groups and pore structure. Simultaneous interactions of π–π conjugation and hydrogen bonding are the primary forces driving IBP adsorption onto PANI/H-BC according to batch experiments. Additionally, pore filling and electrostatic interactions also contribute to the adsorption process. Finally, the fabricated PANI/H-BC composite exhibited rapid, robust adsorption performance for IBP, maintaining stable reusability. This study provides significant insights into the adsorption behavior and mechanism of IBP from aquatic environments by BC-based adsorbents. Future studies should be conducted to investigate the removal of diverse PPCPs using PANI/H-BC accompanied by scale-up studies to evaluate their practical viability for industrial applications.

Table 2 Estimated costs for producing 1 kg of PANI/H-BC

Particular	Sub section	Cost analysis	Amount (USD)
Raw material processing	–	Free collection from Baiyangdian area	0
Preparation of BC from reeds	Drying cost	Hours × unit[a)] × per unit cost[b)] = 24 × 1.4 × 0.071	2.386
	Carbonization cost	Hours ×unit ×per unit cost = 0.5 × 3 × 0.071	0.107
Total cost	–	2.386 + 0.107 + 0.498	2.991

Notes: a) Unit: power of the instrument used. b) Per unit cost: cost of electricity per kilowatt-hour.

Conflict of Interests The authors declare that they have no known competing financial interests or personal relationships that could have appeared to influence the work reported in this paper.

Acknowledgements The authors are grateful for the support of the Key Project of National Natural Science Foundation of China (No. 42330705), the Core Talent Project under the Yanzhao Gold Terrace Attracting Talent Plan (Education Platform) of Hebei Province, China (No. HJZD202507), the Science Research Project of Hebei Education Department, China (No. QN2024216), and the Collaborative Innovation Center for Baiyangdian Basin Ecological Protection and Beijing-Tianjin-Hebei Sustainable Development.

Electronic Supplementary Material Supplementary material is available in the online version of this article at https://doi.org/10.1007/s11783-025-2055-y and is accessible for authorized users.

References

Ayati A, Tanhaei B, Beiki H, Krivoshapkin P, Krivoshapkina E, Tracey C (2023). Insight into the adsorptive removal of ibuprofen using porous carbonaceous materials: a review. Chemosphere, 323: 138241

Bui T X, Choi H (2009). Adsorptive removal of selected pharmaceuticals by mesoporous silica SBA-15. Journal of Hazardous Materials, 168(2−3): 602–608

Chakraborty P, Banerjee S, Kumar S, Sadhukhan S, Halder G (2018a). Elucidation of ibuprofen uptake capability of raw and steam activated biochar of *Aegle marmelos* shell: isotherm, kinetics, thermodynamics and cost estimation. Process Safety and Environmental Protection, 118: 10–23

Chakraborty P, Show S, Banerjee S, Halder G (2018b). Mechanistic insight into sorptive elimination of ibuprofen employing bi-directional activated biochar from sugarcane bagasse: performance evaluation and cost estimation. Journal of Environmental Chemical Engineering, 6(4): 5287–5300

Dey D, Khan P, Biswas R, Saha S, Halder G (2025). Pioneering adsorption-based technological advancements in Ibuprofen remediation: a critical evaluation. Process Safety and Environmental Protection, 196: 106874

Golovina N I, Nechiporenko G N, Zyuzin I N, Lempert D B, Nemtsev G G, Shilov G V, Utenyshev A N, Bozhenko K V (2008). Several aspects of intermolecular interactions between the carbonyl and imine groups in the crystals of compounds containing six-membered heterocycles. Journal of Structural Chemistry, 49(5): 909–916

Guerra P, Kim M, Shah A, Alaee M, Smyth S A (2014). Occurrence and fate of antibiotic, analgesic/anti-inflammatory, and antifungal compounds in five wastewater treatment processes. Science of the Total Environment, 473–474: 235–243

Guo J F, Xiao H H, Zhang J B, Dai C M, Li T Z, Gao M T, Hu J J, Li J X (2024). Characterization of highly stable biochar and its application for removal of phenol. Biomass Conversion and Biorefinery, 14(12): 13311–13321

Herath A, Reid C, Perez F, Pittman C U, Mlsna T E (2021). Biochar-supported polyaniline hybrid for aqueous chromium and nitrate adsorption. Journal of Environmental Management, 296: 113186

Huang M T, Wang M, Yang L M, Wang Z H, Yu H X, Chen K C, Han F, Chen L, Xu C X, Wang L H, et al. (2024). Correction: direct regeneration of spent lithium-ion battery cathodes: from theoretical study to production practice. Nano-Micro Letters, 16(1): 225

Jung C, Boateng L K, Flora J R V, Oh J, Braswell M C, Son A, Yoon Y (2015). Competitive adsorption of selected non-steroidal anti-inflammatory drugs on activated biochars: experimental and molecular modeling study. Chemical Engineering Journal, 264: 1–9

Li Y M, Zhang Y, Zhang Y, Wang G X, Li S Y, Han R M, Wei W (2018). Reed biochar supported hydroxyapatite nanocomposite: characterization and reactivity for methylene blue removal from aqueous media. Journal of Molecular Liquids, 263: 53–63

Lin L, Jiang W B, Xu P (2017). Comparative study on pharmaceuticals adsorption in reclaimed water desalination concentrate using biochar: impact of salts and organic matter. Science of The Total Environment, 601–602: 857–864

Liu W X, Lou T, Wang X J (2023). Enhanced dye adsorption with conductive polyaniline doped chitosan nanofibrous membranes. International Journal of Biological Macromolecules, 242: 124711

Luo Z J, Peng X, Liang W W, Zhou D, Dang C X, Cai W Q (2023). Enhanced adsorption of roxarsone on iron–nitrogen co-doped biochar from peanut shell: synthesis, performance and mechanism. Bioresource Technology, 388: 129762

Mei Y L, Xu J, Zhang Y, Li B, Fan S S, Xu H C (2021). Effect of Fe–N modification on the properties of biochars and their adsorption behavior on tetracycline removal from aqueous solution. Bioresource Technology, 325: 124732

Mondal S, Aikat K, Halder G (2016). Biosorptive uptake of ibuprofen by chemically modified *Parthenium hysterophorus* derived biochar: equilibrium, kinetics, thermodynamics and modeling. Ecological Engineering, 92: 158–172

Mondol M M H, Yoo D K, Jhung S H (2022). Adsorptive removal of carbamazepine and ibuprofen from aqueous solution using a defective Zr-based metal-organic framework. Journal of Environmental Chemical Engineering, 10(6): 108560

Navarathna C M, Karunanayake A G, Gunatilake S R, Pittman C U, Perez F, Mohan D, Mlsna T (2019). Removal of Arsenic(III) from water using magnetite precipitated onto Douglas fir biochar. Journal of Environmental Management, 250: 109429

Ortiz de García S A, Pinto Pinto G, García-Encina P A, Irusta-Mata R (2014). Ecotoxicity and environmental risk assessment of pharmaceuticals and personal care products in aquatic environments and wastewater treatment plants. Ecotoxicology, 23(8): 1517–1533

Rafiqi F A, Majid K (2017). Sequestration of methylene blue (MB) dyes from aqueous solution using polyaniline and polyaniline–nitroprusside composite. Journal of Materials Science, 52(11): 6506–6524

Ren W, Xiong L L, Nie G, Zhang H, Duan X G, Wang S B (2020). Insights into the electron-transfer regime of peroxydisulfate activation on carbon nanotubes: the role of oxygen functional groups. Environmental Science & Technology, 54(2): 1267–1275

Schlautman M A, Yim S, Carraway E R, Lee J H, Herbert B E (2004). Testing a surface tension-based model to predict the salting out of polycyclic aromatic hydrocarbons in model environmental solutions. Water Research, 38(14−15): 3331–3339

Show S, Mukherjee S, Devi M S, Karmakar B, Halder G (2021). Linear and non-linear analysis of Ibuprofen riddance efficacy by *Terminalia catappa* active biochar: equilibrium, kinetics, safe disposal, reusability and cost estimation. Process Safety and Environmental Protection, 147: 942–964

Shyamala S, Kalaiarasi S, Karpagavinayagam P, Vedhi C, Muthuchudarkodi R R (2022). Electrochemical studies and electrocatalytic applications of Zirconia-Polyaniline nano-composite. Journal of Electroanalytical Chemistry, 923: 116834

Wang J H, Ji Y F, Ding S L, Ma H R, Han X J (2013). Adsorption and desorption behavior of tannic acid in aqueous solution on polyaniline adsorbent. Chinese Journal of Chemical Engineering, 21(6): 594–599

Xi H, Min F L, Yao Z H, Zhang J F (2023). Facile fabrication of dolomite-doped biochar/bentonite for effective removal of phosphate from complex wastewaters. Frontiers of Environmental Science & Engineering, 17(6): 71

Xiong T, Yuan X Z, Wang H, Wu Z B, Jiang L B, Leng L J, Xi K F, Cao X Y, Zeng G M (2019). Highly efficient removal of diclofenac sodium from medical wastewater by Mg/Al layered double hydroxide-poly(m-phenylenediamine) composite. Chemical Engineering Journal, 366: 83–91

Yang L M, Feng Y F, Wang C Q, Fang D F, Yi G P, Gao Z, Shao P H, Liu C L, Luo X B, Luo S L (2022). Closed-loop regeneration of battery-grade $FePO_4$ from lithium extraction slag of spent Li-ion batteries *via* phosphoric acid mixture selective leaching. Chemical Engineering Journal, 431: 133232

Yang L M, Gao Z, Liu T, Huang M T, Liu G Z, Feng Y F, Shao P H, Luo X B (2023a). Direct electrochemical leaching method for high-purity lithium recovery from spent lithium batteries. Environmental Science & Technology, 57(11): 4591–4597

Yang L M, Tu Y Y, Li H Y, Zhan W L, Hu H Q, Wei Y, Chen C L, Liu K T, Shao P H, Li M, et al. (2023b). Fluorine-rich supramolecular nano-container crosslinked hydrogel for lithium extraction with super-high capacity and extreme selectivity. Angewandte Chemie International Edition, 62(38): e202308702

Yea Y, Kim G, Wang D J, Kim S, Yoon Y, Elanchezhiyan S S, Park C M (2022). Selective sequestration of perfluorinated compounds using polyaniline decorated activated biochar. Chemical Engineering Journal, 430: 132837

Zhang H, Li J H, Huang X Y, Duan X M, Yue R R, Xu J K (2024). Lamellar polyaniline-modified reduced graphene oxide loaded electron-rich Pd nanoparticles for highly efficient electrooxidation of C2 alcohols. Fuel, 369: 131781

Zhang K K, Sun P, Faye M C A S, Zhang Y R (2018). Characterization of biochar derived from rice husks and its potential in chlorobenzene degradation. Carbon, 130: 730–740

Zhao T S, Liu X M, Huai L K, Feng R, Yan T, Xu W Y, Zhao Y X (2024). Fabrication of the TiO_2/Ti_3C_2 loaded ceramic membrane targeting for photocatalytic degradation of PPCPs: ciprofloxacin, tetracycline, and ibuprofen. Frontiers of Environmental Science & Engineering, 18(10): 123